Supporting Information

Nanocrystallization of Triazolate-Based Metal–Organic Frameworks Boosting Photocatalytic Hydrogen Peroxide Production

Shujun Xing,[a] *Rundong Chen,*[a] *Yuan Gu,*[a] *Huimin Cheng,*[a] *Chenxi Li,*[a] *Kun Fan,*[a,c,]* *Bingquan Xia,*[a] *Shantang Liu*[a,c,]* and Chengliang Wang[b,]*

[a] School of Chemistry and Environmental Engineering, Key Laboratory for Green Chemical Process of Ministry of Education, Wuhan Institute of Technology, Wuhan 430073, P. R. China.

[b] School of Integrated Circuits, State Key Laboratory of New Textile Materials and Advanced Processing, Key Laboratory of Material Chemistry for Energy Conversion and Storage (Ministry of Education), Huazhong University of Science and Technology, Wuhan 430074, P. R. China.

[c] Hubei Three Gorges Lab, Yichang 443000, P. R. China

* *Corresponding authors.*

Experimental section

Characterization

Scanning electron microscopy (SEM) images were acquired using a ZEISS Gemini 300 electron microscope. Powder X-ray diffraction (PXRD) patterns were collected at room temperature on an X'Pert³ Powder diffractometer using Cu Kα radiation (λ = 1.5406 Å). Single-crystal X-ray diffraction (SCXRD) data were collected on an XtaLAB PRO MM007HF diffractometer (Rigaku, Japan). Fourier transform infrared (FT-IR) spectra were recorded in transmission mode (KBr pellets) on a Nicolet IS50 spectrometer. Thermogravimetric analysis (TGA) was performed on a Pyris 1 thermogravimetric analyzer under a continuous nitrogen flow. Measurements were conducted from 30 to 800 °C at a heating rate of 10 °C/min. Solid UV-Vis absorption spectra were recorded using a Shimadzu SolidSpec-3700 spectrophotometer. Steady-state photoluminescence (PL) spectra were measured on a Hitachi F-4600 fluorescence spectrophotometer. Time-resolved photoluminescence (TRPL) decay profiles were acquired using an Edinburgh Instruments FLS1000 fluorescence lifetime spectrophotometer. X-ray photoelectron spectroscopy (XPS) analysis was performed on a Thermo Fisher Scientific ESCALAB 250Xi spectrometer to monitor binding energy shifts before and after light illumination. In situ electron paramagnetic resonance (EPR) spectra were recorded on a Bruker EMXnano spectrometer under xenon lamp illumination. In situ diffuse reflectance infrared Fourier transform spectroscopy (DRIFTS) measurements were carried out on a Nicolet IS50 spectrometer. The Cd content was determined using an Agilent 7800 inductively coupled plasma mass spectrometer (ICP-MS).

Photoelectrochemical and electrochemical tests

Photoelectrochemical measurements were performed using a CHI760E electrochemical workstation. A standard three-electrode configuration was employed, consisting of a working electrode (FTO glass coated with the sample), a platinum foil counter electrode, and a saturated Ag/AgCl reference electrode. The electrolyte was a 0.5 M Na_2SO_4 aqueous solution. A 300 W xenon lamp (PLS-SXE 300+) was used as the simulated solar light source. The working electrode was prepared by mixing 5 mg of the synthesized sample with 50 μL deionized water, 2 mL ethanol, and 50 μL Nafion solution to form a homogeneous slurry. 20 μL of this slurry was drop-cast onto a pre-cleaned FTO glass substrate (1 cm × 1 cm) and dried in a vacuum oven at 80 °C for 2 h. Current-time (i-t) curves were conducted at a constant potential of 0.5 V (vs. Ag/AgCl) under intermittent light irradiation. Electrochemical impedance spectroscopy (EIS) was performed at –0.5 V (vs. Ag/AgCl) under continuous illumination. The Nyquist plots were recorded over a frequency range of 0.1 Hz to 100 kHz with an AC amplitude of 5 mV.

Photocatalytic performance testing

In the photocatalytic reaction, an AC90 230 V ultraviolet lamp was used as the light source, with a wavelength of 420 nm. The light power density at the liquid surface of the reactor was measured to be 608 mW/cm² using PL-MW2000Q high-intensity optical power meter. The temperature was maintained at 25°C during the reaction by a constant temperature device. The photocatalytic H_2O_2 production was evaluated under visible-light irradiation (λ = 420 nm). In a typical test, 5 mg of catalyst was dispersed in 20 mL of pure water by 5 min of sonication in the dark. The suspension was then purged with O_2 for 30 min (dark) before irradiation. The reaction proceeded under visible light with continuous stirring for 1 h. The catalyst was removed by filtration through a 0.22 μm nylon syringe filter. The H_2O_2 concentration in the clear filtrate was quantified spectrophotometrically at 350 nm using a pre-calibrated standard curve. All photocatalytic H_2O_2 production experiments in this study were conducted in triplicate (n = 3) to ensure reliability and reproducibility. The data are presented as the average of three independent runs, and the error bars indicate the standard deviation.

Table S1. Crystallographic Data for Cd-BTBQ.

Cd-BTBQ	
Empirical formula	$CdC_6H_4N_6O_4$
Formula weight	336.55
Temperature/K	293(2)
Crystal system	monoclinic
Space group	$P2_1/n$
a/Å	6.54470(10)
b/Å	10.12850(10)
c/Å	13.11640(10)
α/°	90
β/°	93.9710(10)
γ/°	90
Volume/Å^3	867.372(17)
Z	4
ρ_{calc}g/cm^3	2.577
μ/mm^{-1}	20.428
F(000)	648.0
Crystal size/mm^3	0.08 × 0.06 × 0.05
Radiation	CuKα (λ = 1.54178)
2Θ range for data collection/°	11.046 to 148.128
Index ranges	$-7 \leq h \leq 8$, $-12 \leq k \leq 12$, $-16 \leq l \leq 8$
Reflections collected	9278
Independent reflections	1746 [R_{int}= 0.0389, R_{sigma}= 0.0246]
Data/restraints/parameters	1746/0/156
Goodness-of-fit on F^2	0.844
Final R indexes [I>=2σ (I)]	R_1= 0.0270, wR_2= 0.0893
Final R indexes [all data]	R_1= 0.0276, wR_2= 0.0907
CCDC number	2495951

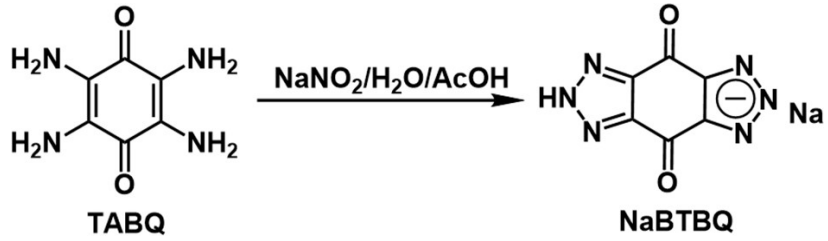

Scheme S1. The synthetic routes for **NaBTBQ**.

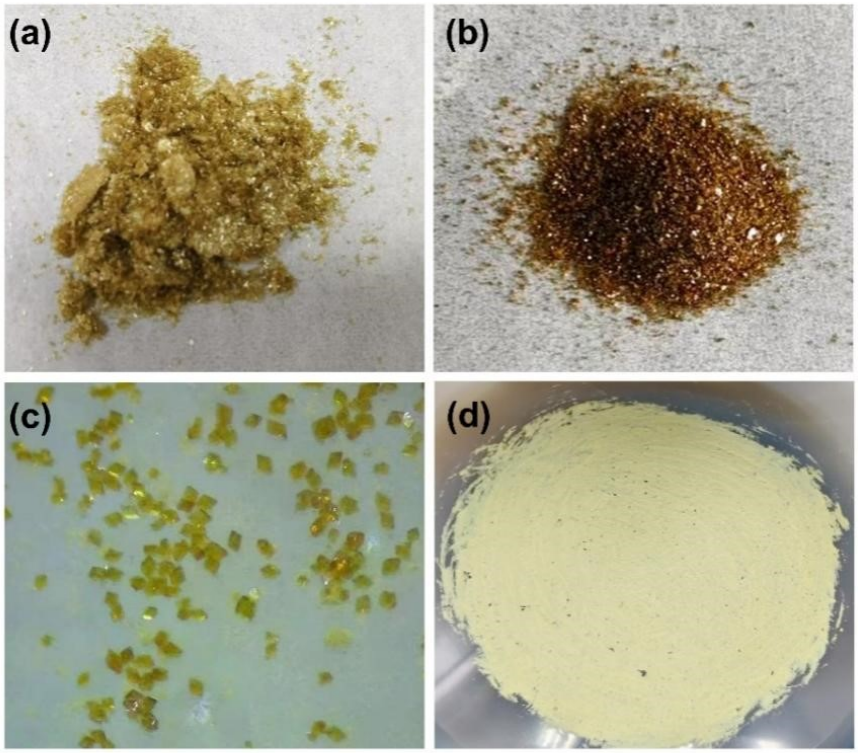

Figure S1. Optical microscopy image of (a) the NaBTBQ ligands, (b, c) Cd-BTBQ-C and (d) Cd-BTBQ-N.

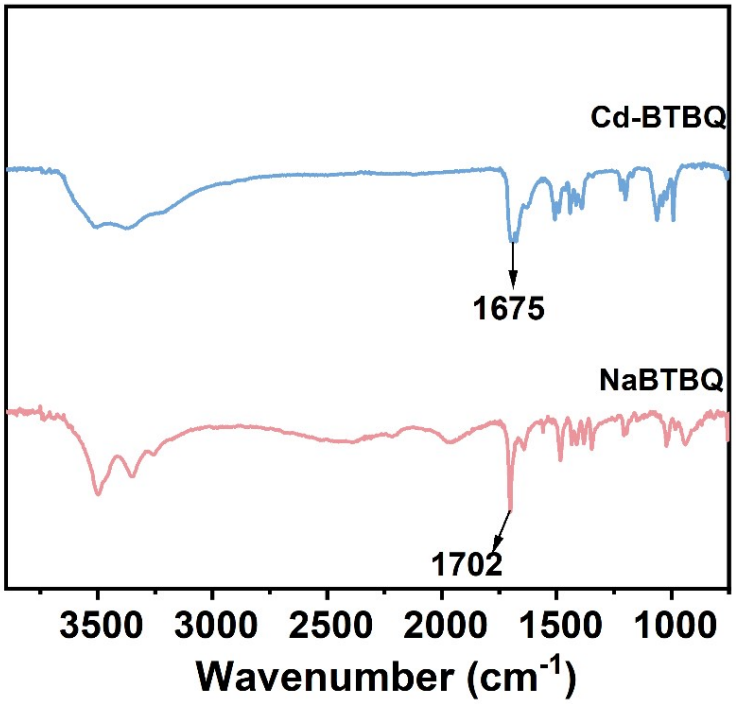

Figure S2. FTIR spectra of NaBTBQ and Cd-BTBQ.

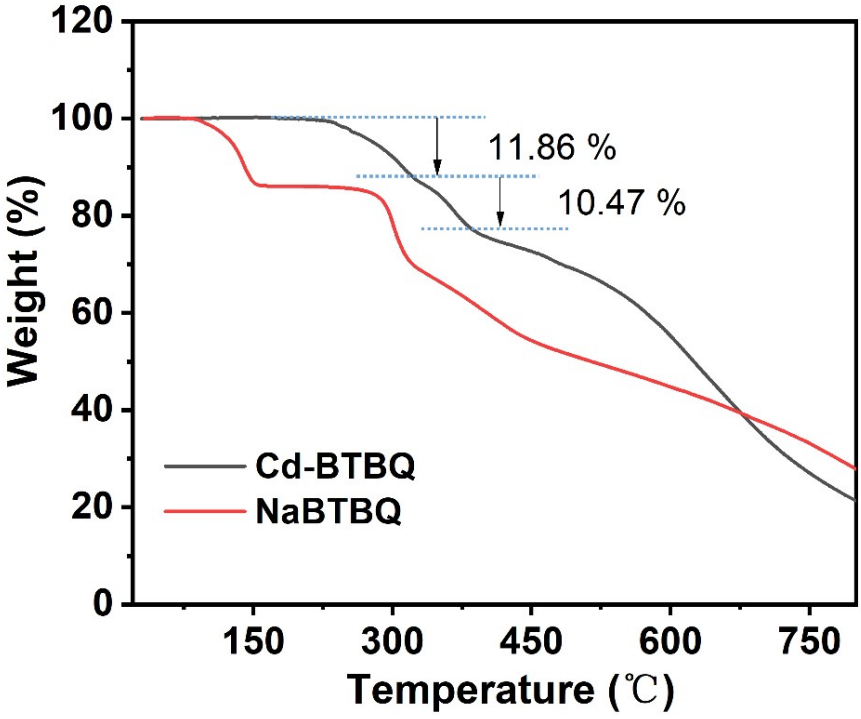

Figure S3. Thermogravimetric analysis (TGA) curve of NaBTBQ and Cd-BTBQ-C.

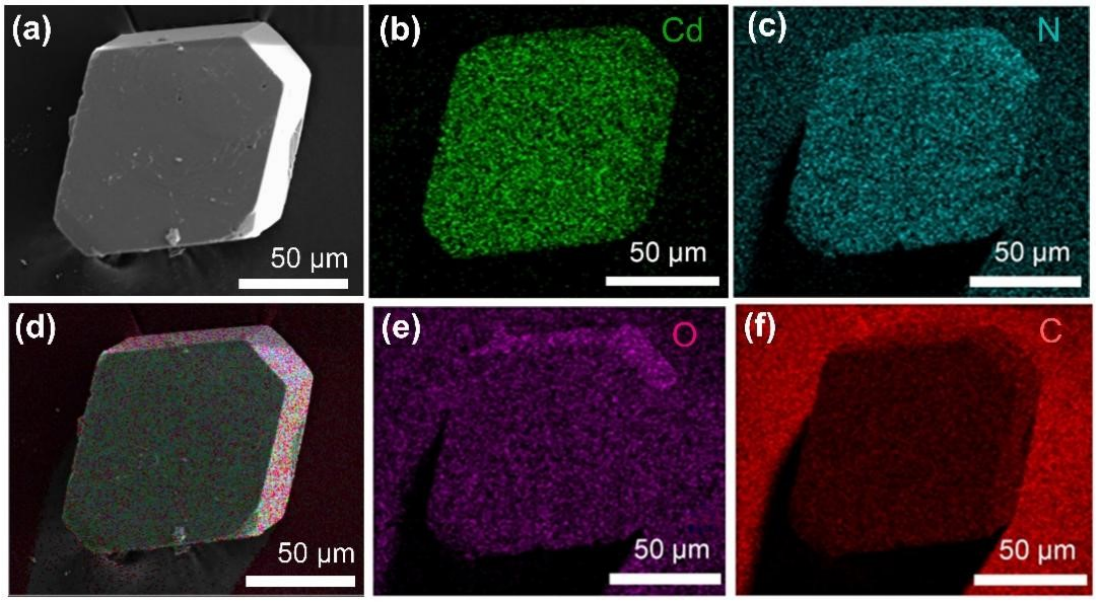

Figure S4. Energy dispersive X-ray spectrum (EDS-mapping) of Cd-BTBQ-C, which indicates that the elements are evenly distributed in the material.

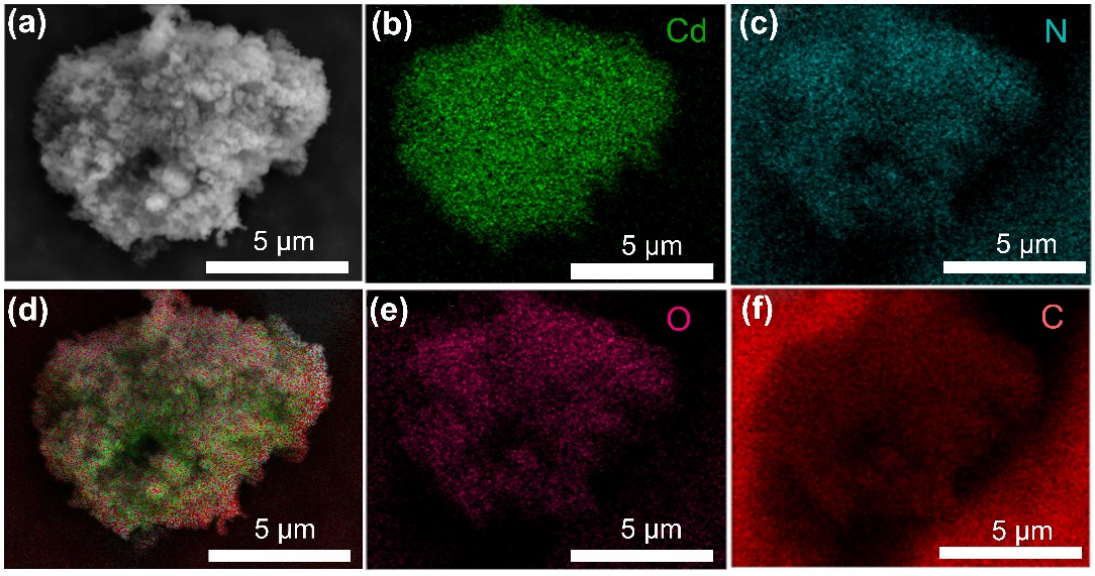

Figure S5. Energy dispersive X-ray spectrum (EDS-mapping) of Cd-BTBQ-N nanosphere, which indicates that the elements are evenly distributed in the material.

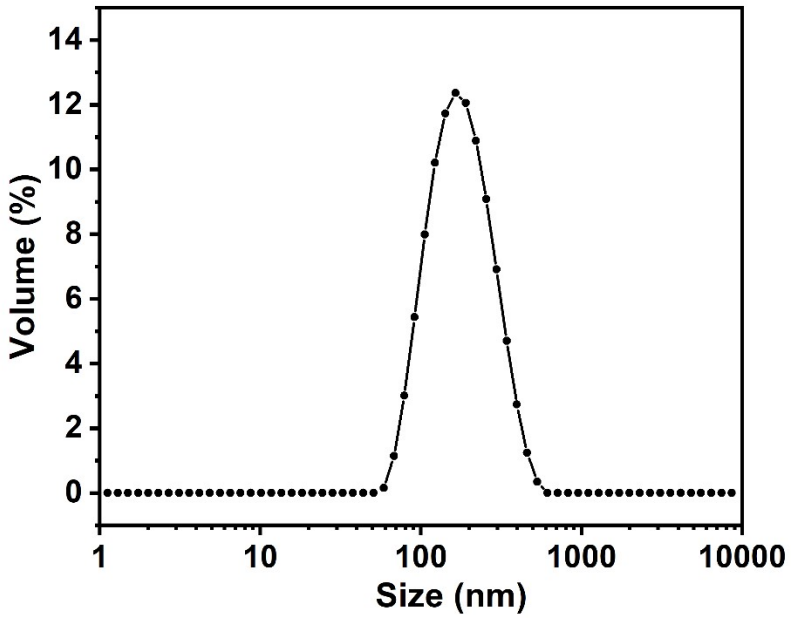

Figure S6. Dynamic light scattering (DLS) measurements of Cd-BTBQ-N. The sample exhibited a Z-average hydrodynamic diameter of 162.8 nm with a polydispersity index (PDI) of 0.19.

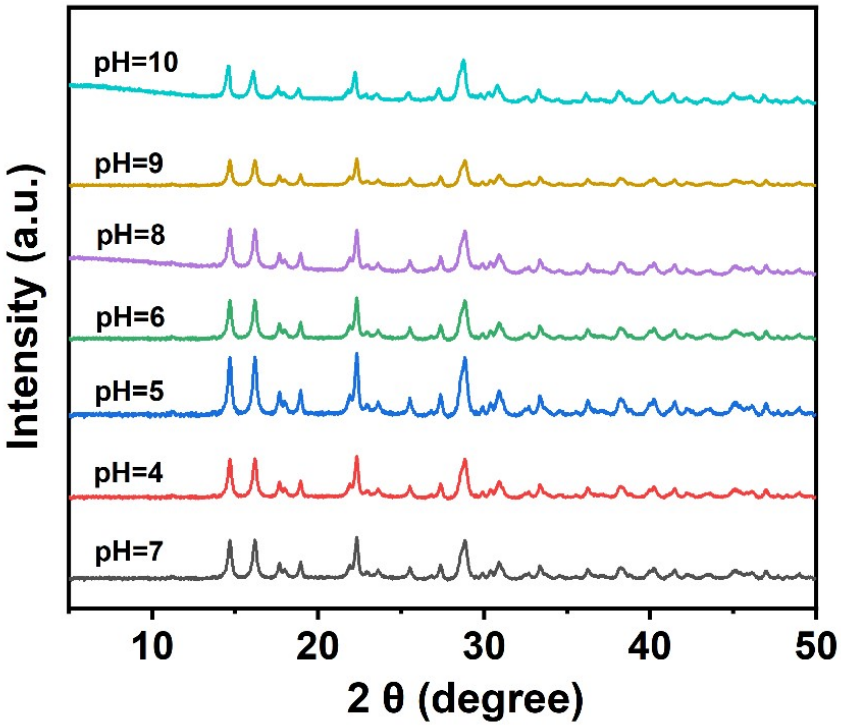

Figure S7. PXRD patterns of Cd-BTBQ-N after two days of immersion in aqueous solutions with different pH values. The negligible changes in the diffraction patterns underscores the good stability of Cd-BTBQ-N.

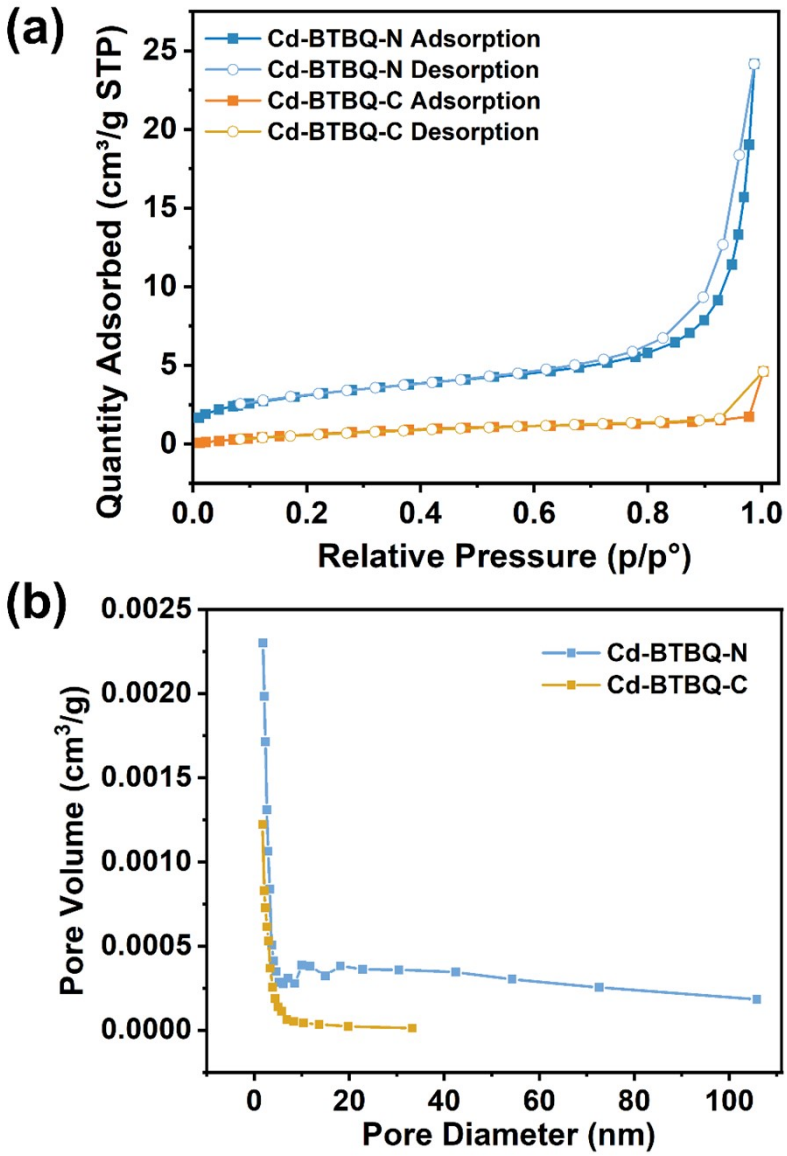

Figure S8. (a) N_2 adsorption-desorption isotherms and (b) pore size distributions of Cd-BTBQ-C and Cd-BTBQ-N.

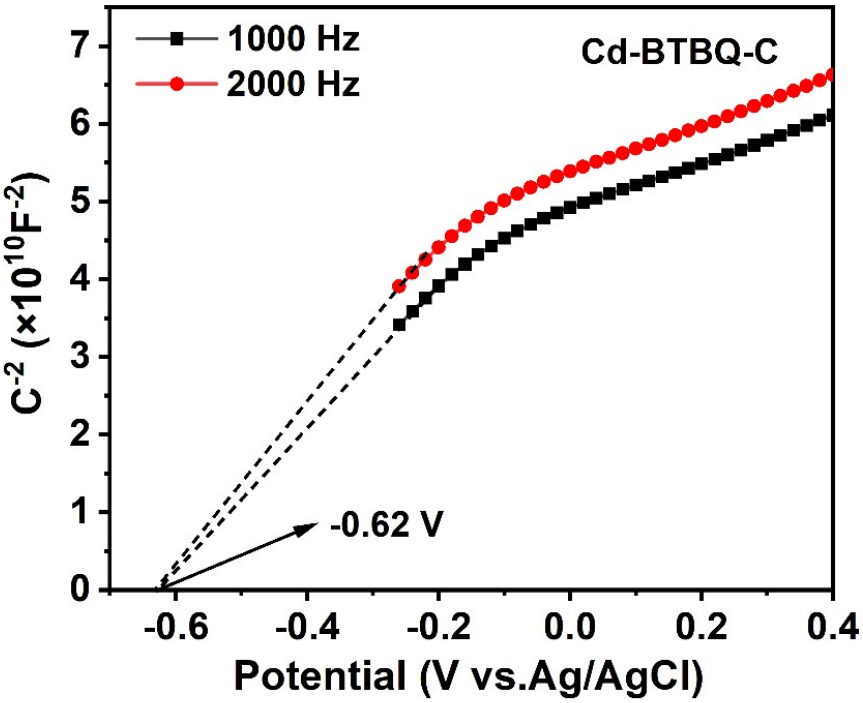

Figure S9. Mott-Schottky plot of Cd-BTBQ-C.

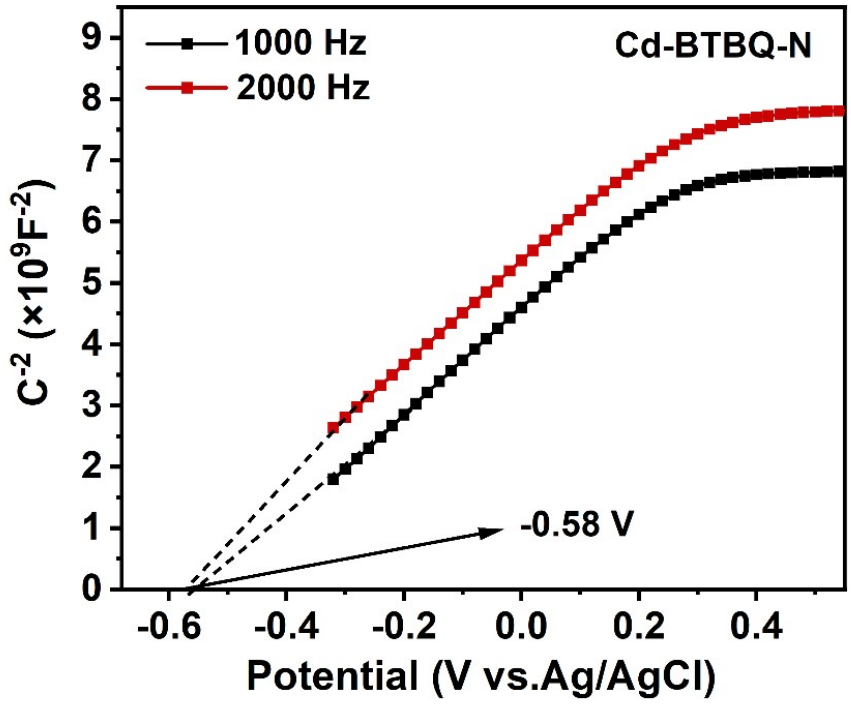

Figure S10. Mott-Schottky plot of Cd-BTBQ-N.

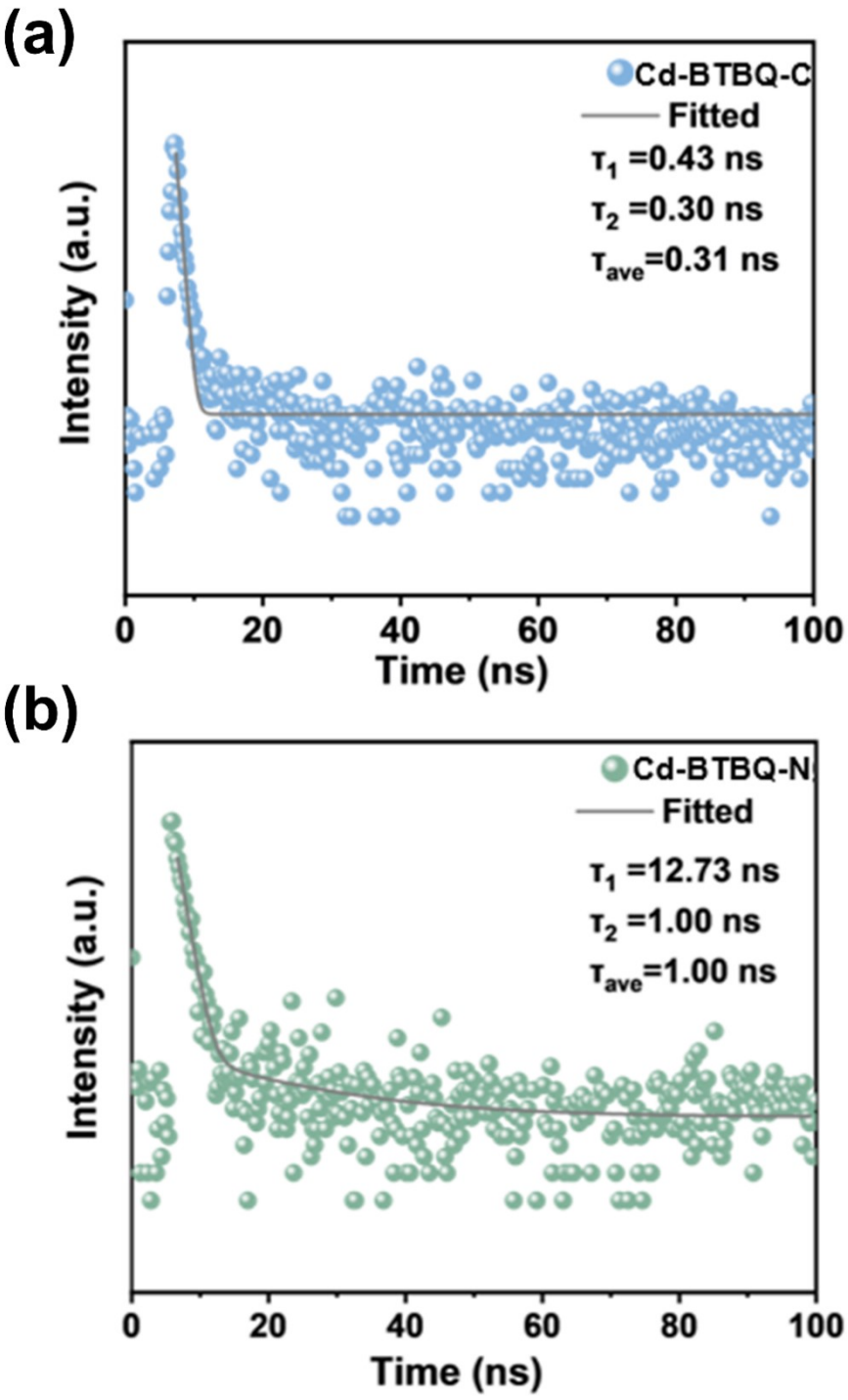

Figure S11. Time-resolved fluorescence decay curves of (a) Cd-BTBQ-C and (b) Cd-BTBQ-N.

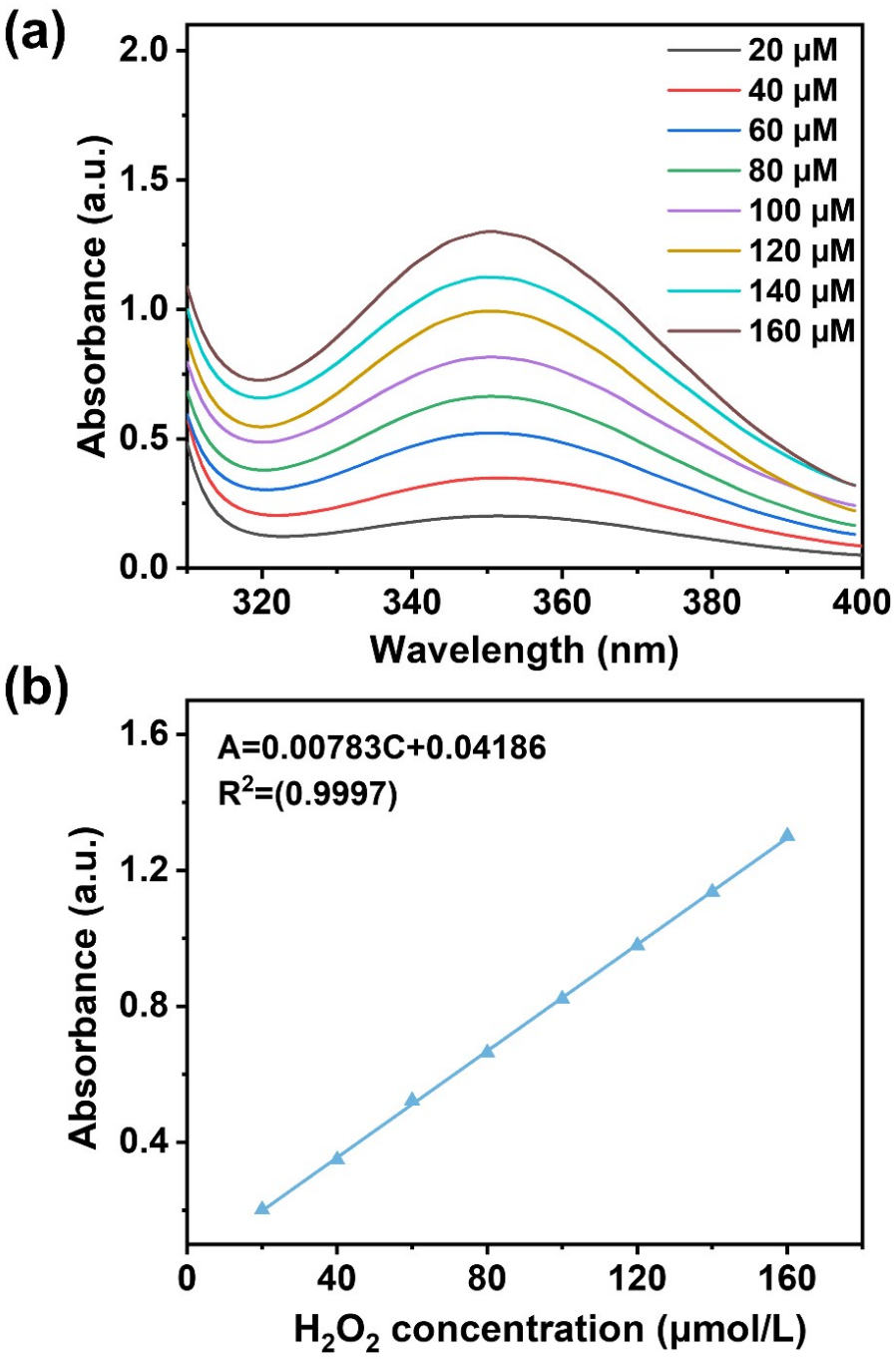

Figure S12. (a) Absorbance curves at different H_2O_2 concentrations; (b) Calibration curve for quantifying photocatalytic H_2O_2 yields.

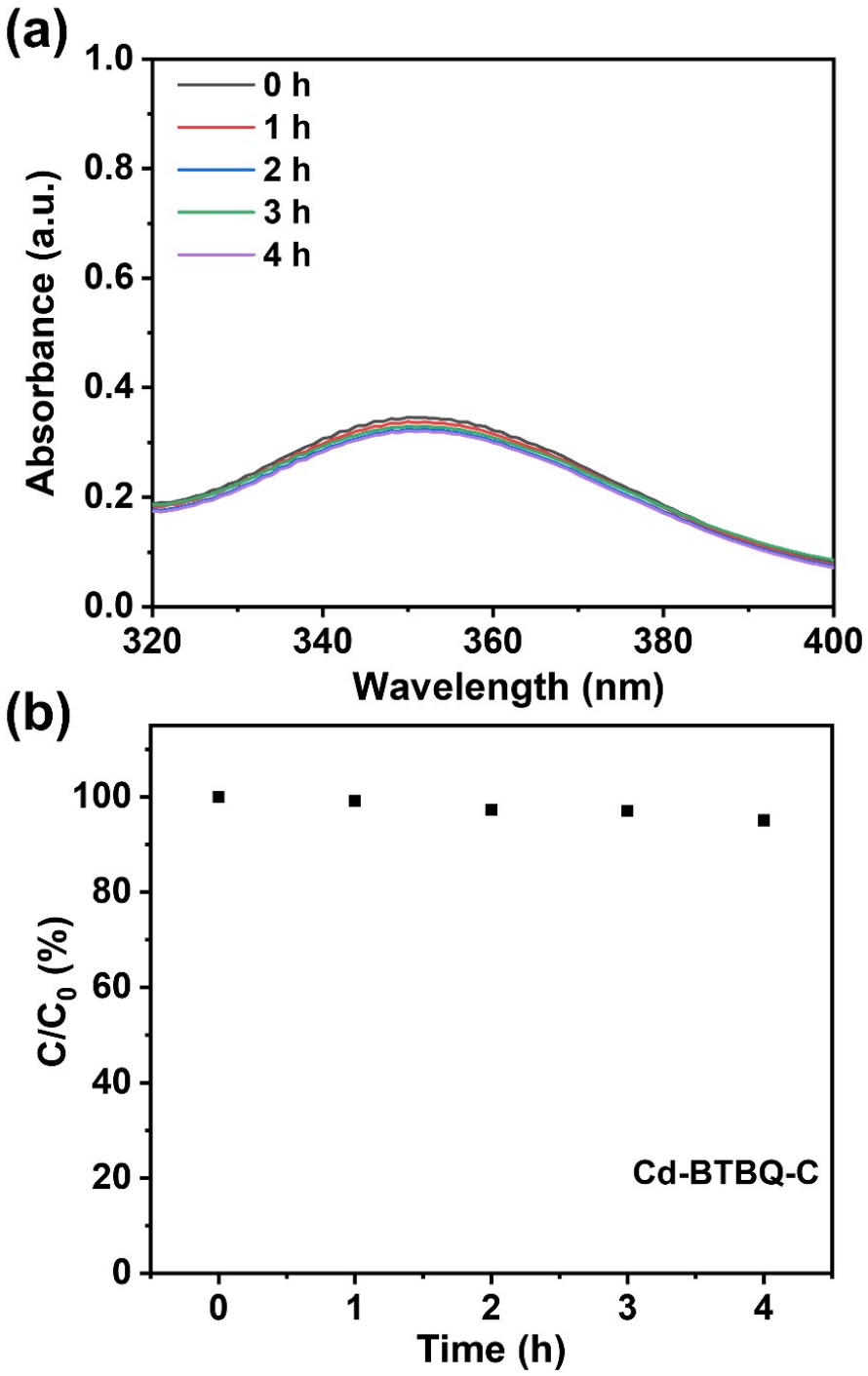

Figure S13. Time course of H_2O_2 decomposition test using Cd-BTBQ-C in the dark. (a) Absorbance curves (b) The time-dependent changes in hydrogen peroxide concentration over 4 h.

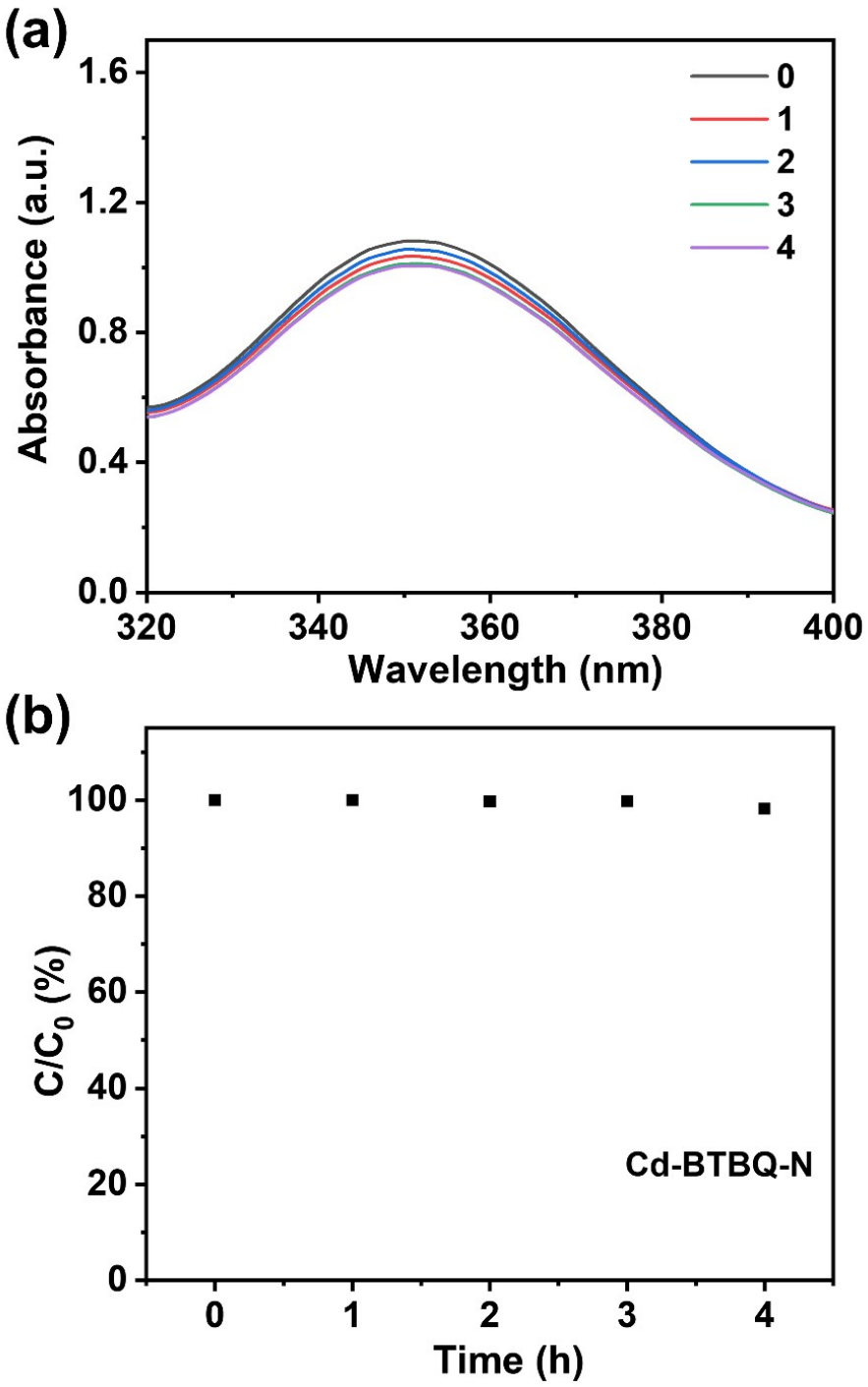

Figure S14. Time course of H_2O_2 decomposition test using Cd-BTBQ-C in the dark. (a) Absorbance curves (b) The time-dependent changes in hydrogen peroxide concentration over 4 h.

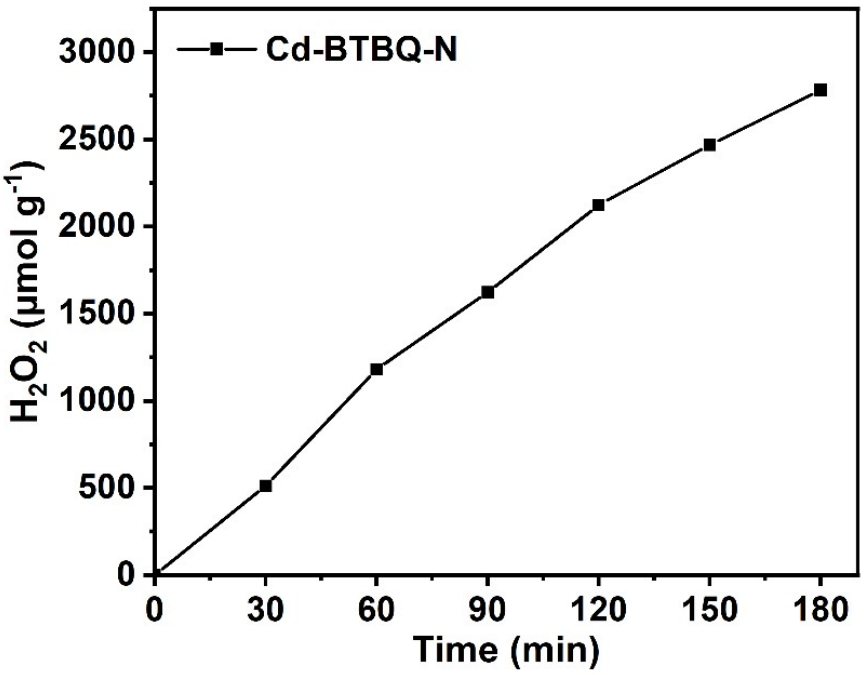

Figure S15. Photocatalytic H_2O_2 production by Cd-BTBQ-N in pure water over 3 h.

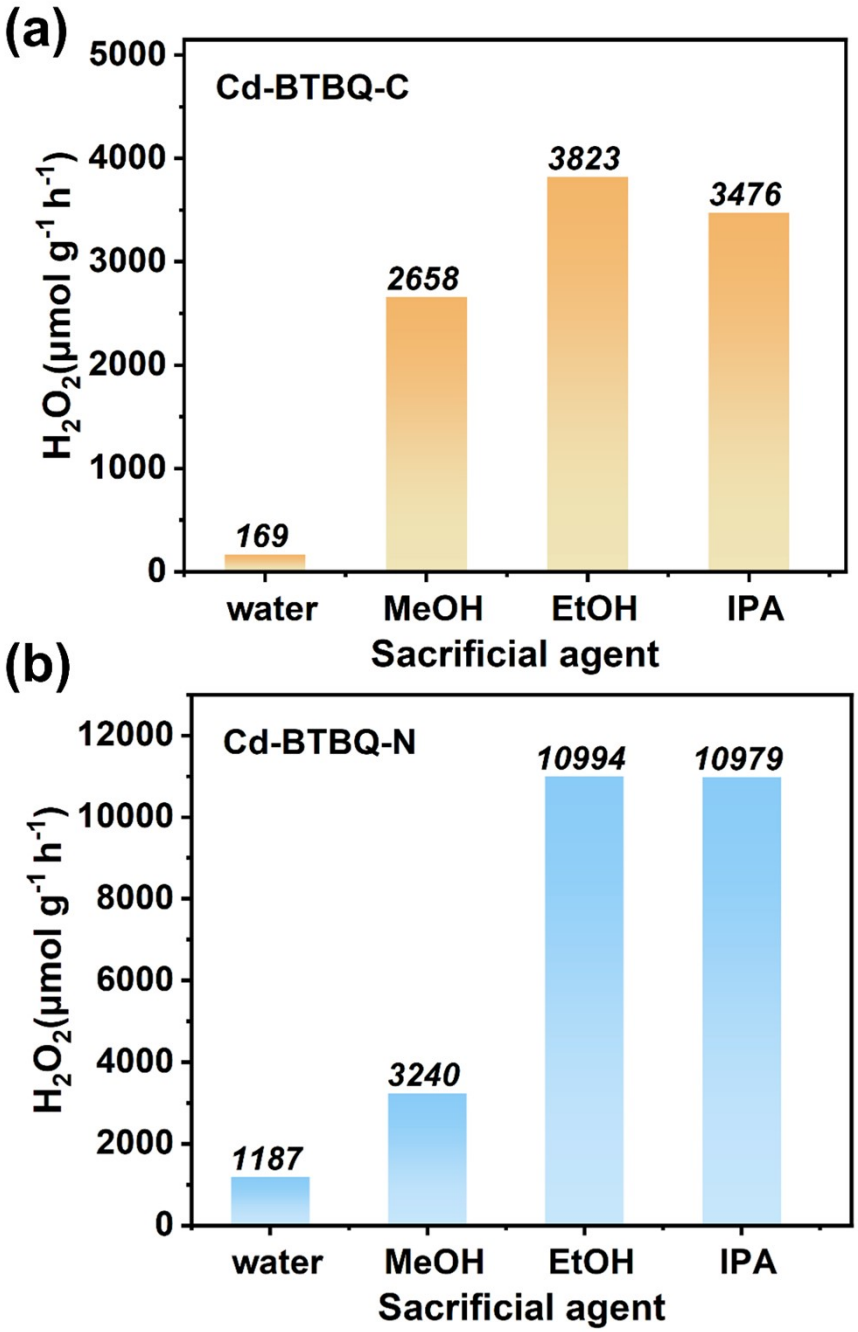

Figure S16. The photoactivity of (a) Cd-BTBQ-C and (b) Cd-BTBQ-N with different scavengers (H_2O, MeOH, EtOH, and IPA).

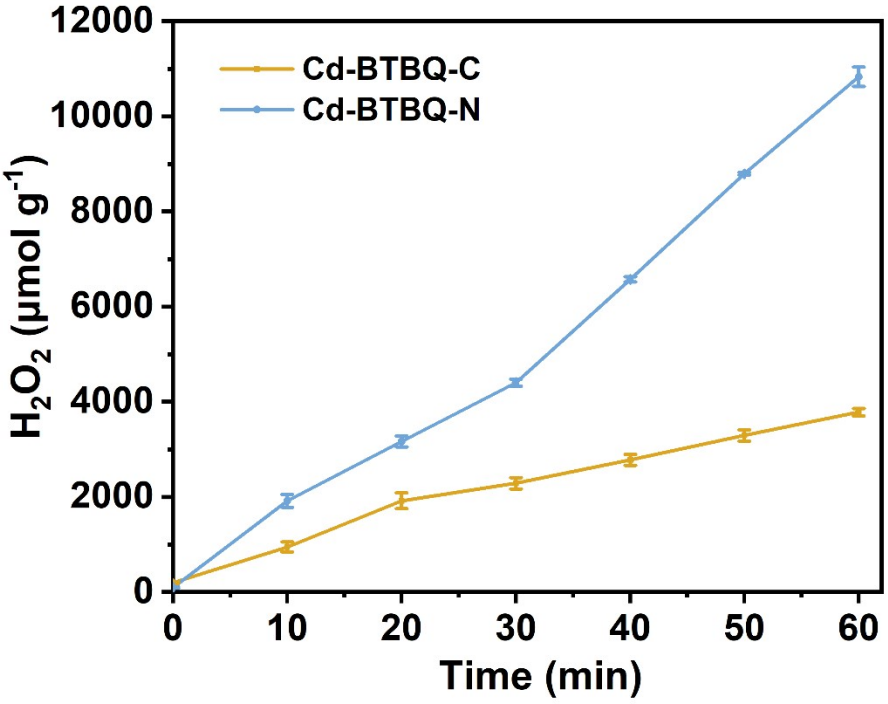

Figure S17. Photocatalytic H_2O_2 production of Cd-BTBQ-C and Cd-BTBQ-N in ethanol/water (1:9 v/v).

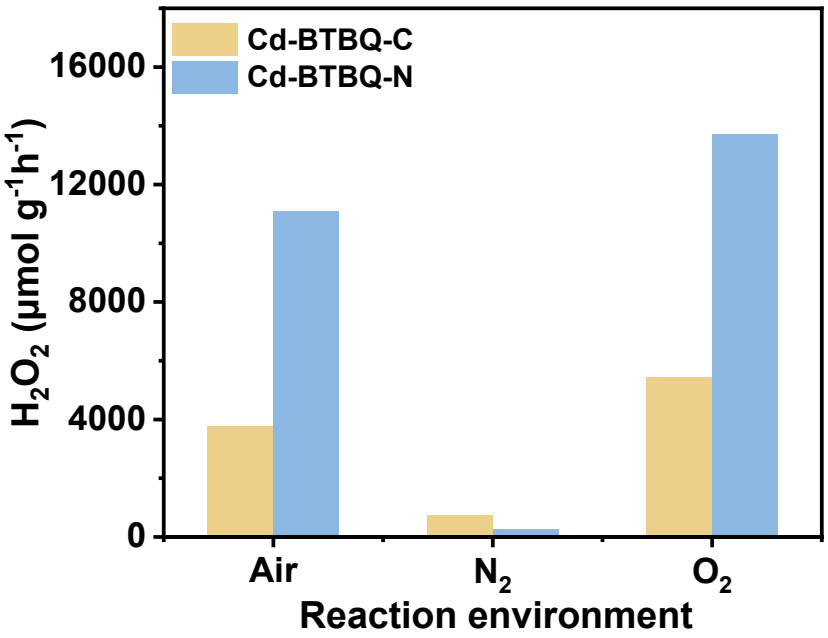

Figure S18. H_2O_2 evolution with Cd-BTBQ-C and Cd-BTBQ-N using ethanol as a sacrificial agent (under air, N_2, or O_2).

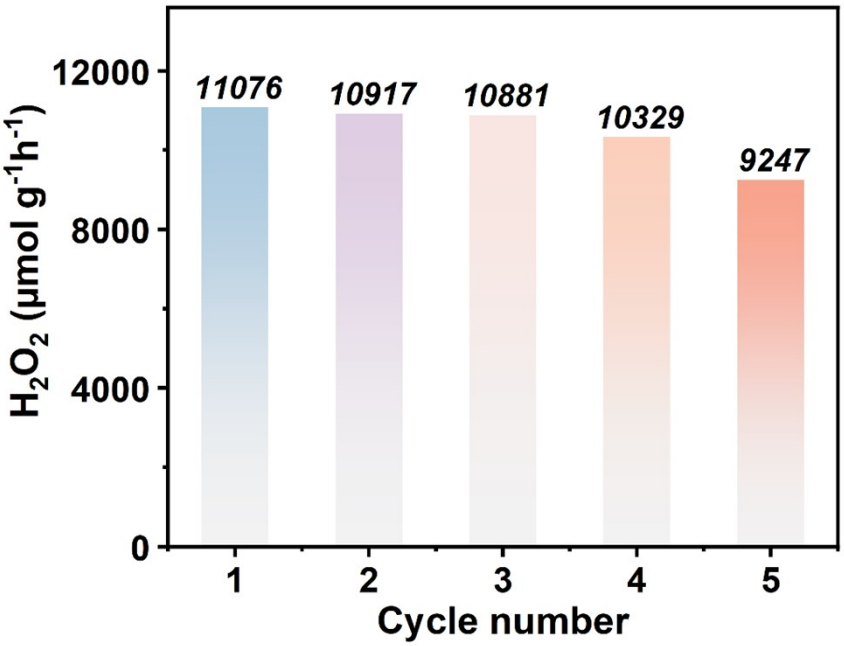

Figure S19. Cyclability test of Cd-BTBQ-N for H_2O_2 production in ethanol/water (1:9 v/v).

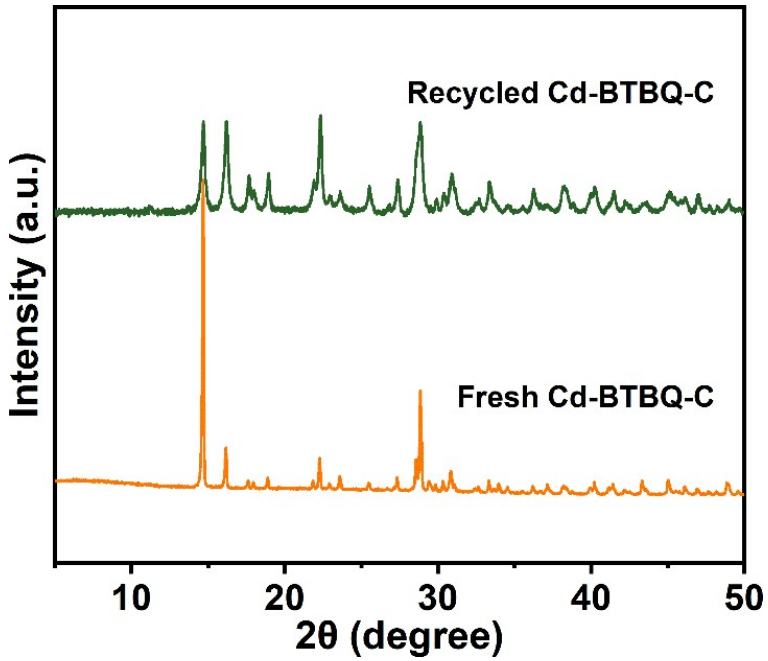

Figure S20. Comparison of PXRD patterns of Cd-BTBQ-C before and after 5 cycles of light irradiation.

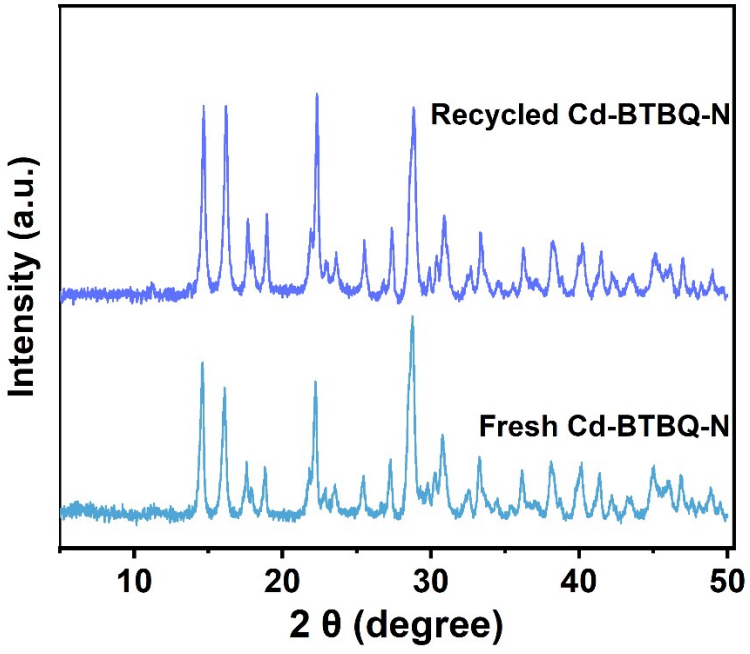

Figure S21. Comparison of PXRD patterns of Cd-BTBQ-N before and after 5 cycles of light irradiation.

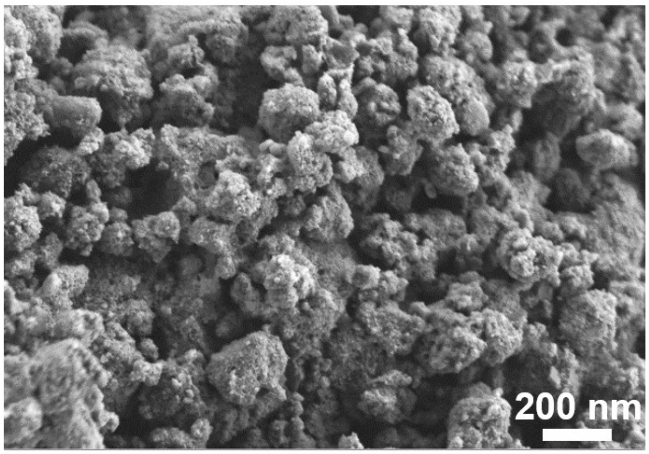

Figure S22. SEM images of Cd-BTBQ-N after 5 photocatalytic cycles.

Table S2. The ICP results of Cd-BTBQ-N after photocatalytic reaction (filter liquor).

Sample	Cd^{2+} (μg/L)	Dissolution (%)
Cd-BTBQ-N Powder (5mg/20mL)	1.900	0.00227
Cd-BTBQ-N Film (5mg/20mL)	0.303	0.00036

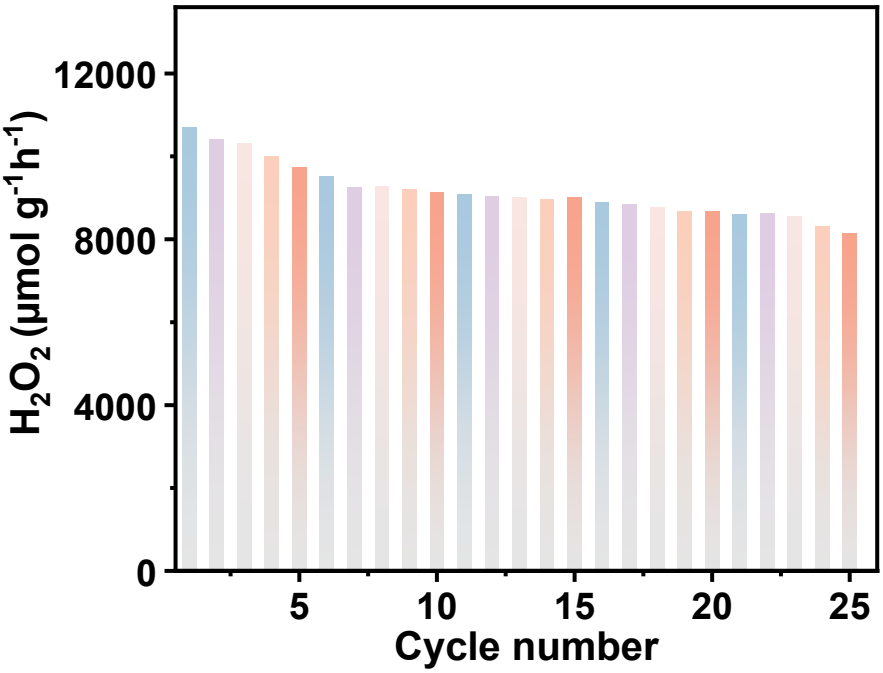

Figure S23. Long-term stability of Cd-BTBQ-N for photocatalytic H_2O_2 production in in ethanol/water (1:9 v/v).

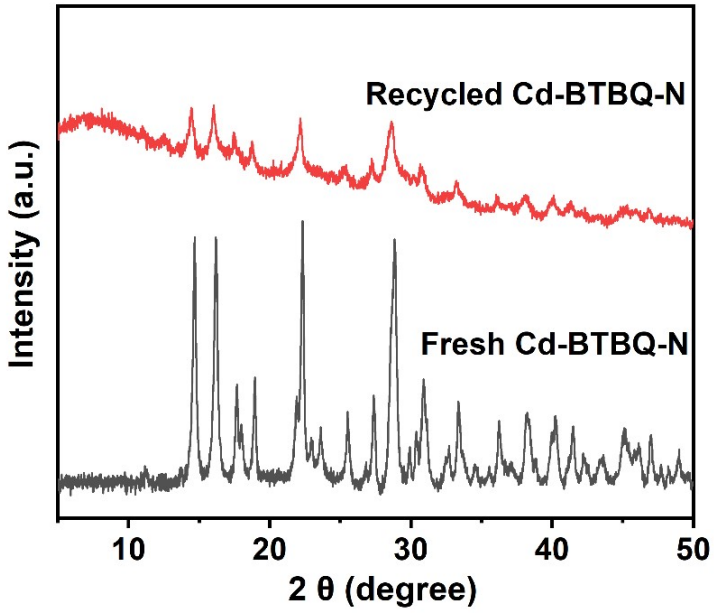

Figure S24. Comparison of PXRD patterns of Cd-BTBQ-N before and after 25 cycles of light irradiation.

Table S3. Comparison of the photocatalytic H_2O_2 production over MOF-based photocatalysts without sacrificial agent.

Catalyst	Light	Sacrificial agent	Gas atmosphere	Production rate (umol g^{-1} h^{-1})	Production pathway	Ref
NH_2-MIL-111	Vis	No	O_2	917	ORR, WOR	1
aMIL	Vis	No	O_2	926	Indirect ORR	2
Al-TCPP(10-X)-$TBAP_yX$	Vis	No	O_2	130	ORR, WOR	3
C_3N_4/ZIF-8	Vis	No	Air	2641	ORR, WOR	4
C_3N_4/Ni-CAT	Vis	No	O_2	1801	Indirect ORR	5
NH_2-MIL-101(Fe)@MCN/Bi_2O_3	Vis	No	O_2	656	Indirect ORR	6
$ZnIn_2S_4$/MIL-88B(Fe)–NH_2	Vis	No	Air	504	Indirect ORR	7
UiO-67-$(NH_2)_2$	λ =427 nm	No	O_2	480	Direct ORR	8
JNM-24	Vis	No	O_2	382	ORR, WOR	9
Cd-BTBQ-C	**420 nm UV lamp**	**No**	**Air**	**169**	**ORR**	**This work**
			O_2	**265**		
Cd-BTBQ-N			**Air**	**1187**	**ORR, WOR**	
			O_2	**1452**		

Table S4. Comparison of the photocatalytic H_2O_2 production over MOF-based photocatalysts with sacrificial agent.

Catalyst	Light	Sacrificial agent	Gas atmosphere	Production rate (umol g^{-1} h^{-1})	Production pathway	Ref
UiO-66	Simulated UV light	Isopropanol	O_2	314	Indirect ORR	10
UiO-66-B	Solar	Isopropanol	O_2	1002	Indirect ORR	10
MIL-125-xL2	Vis	Triethanolamine	O_2	1654	Indirect ORR	11
NTU-9	Vis	Triethanolamine	O_2	3505	Indirect ORR	12
Ni/MIL-125-NH_2	Vis	Triethanolamine	O_2	1617	Indirect ORR	13
MIL-125-NH_2(TiO_2)/Ti_3C_2	Vis	Isopropanol	O_2	5560	ORR, WOR	14
$Bi_2O_2CO_3$/Bi-MOF	> 420 nm	Ethanol	Air	280	Direct ORR	15
OPA/MIL-125-NH_2	Vis	Benzyl alcohol	O_2	1950	Indirect ORR	16
OPA/$Zr_{100-x}Ti_x$-MOF	Vis	Benzyl alcohol	O_2	9700	Indirect ORR	17
Pd/UiO-66-NH_2	Vis	Isopropanol	O_2	10,400	ORR	18
Defective UiO-66	UV–vis	Triethanolamine	O_2	121	Indirect ORR	19
CP-5	Vis	Ethanol	O_2	5970	Direct ORR	20
PdNPs/A-aUiO	Vis	Isopropanol	Air	140	ORR	21
MAF-6	> 400 nm	Isopropanol	O_2	1005	ORR WOR	22
Cd-BTBQ-C	**420 nm UV lamp**	**Ethanol**	**Air**	**3823**	**ORR**	**This work**
			O_2	**5436**		
Cd-BTBQ-N			**Air**	**11076**	**ORR, WOR**	
			O_2	**13712**		

Table S5. Comparison of the photocatalytic H_2O_2 production over with other nanomaterials.

Catalyst	Light	Sacrificial agent	Gas atmosphere	Production rate (umol g^{-1} h^{-1})	Production pathway	Ref
Al-P(bulk)	λ > 420 nm	No	O_2	17.6 (umol L^{-1} h^{-1})	/	23
Al−P(layered)	λ > 420 nm	No	O_2	25.4 (umol L^{-1} h^{-1})	ORR WOR	23
Pd/Zn@rGO/ MO:$BiVO_4$	λ > 400 nm	Ethanol	O_2	3936	WOR	24
Al-TCPP-Sb	Xe lamp	No	O_2	663.2	Indirect ORR	25
S_v-ZIS	λ > 420 nm	No	O_2	1706.4	ORR	26
DDCN	λ > 420 nm	Ethanol	O_2	1031	ORR	27
MTP_{Li-K}	λ > 420 nm	IPA	Air	2807	ORR	28
P-CoNi/ZIS	Xe lamp	No	O_2	1105.5	ORR	29
LCM_{96}	visible light	No	O_2	203.5 (umol L^{-1})	ORR	30
K-CZ-2	LED light	benzyl alcohol	O_2	7800	ORR	31
g-C_3N_4@CoO_2	Xe lamp	No	O_2	412.7	ORR	32
B-CsCN-Ns	Xe lamp	Ethanol	O_2	113	ORR	33
GCN-B	Xe lamp	Ethanol	O_2	19	ORR	33
Cd-BTBQ-N	**420 nm UV lamp**	**No**	**Air**	**1187**	**ORR, WOR**	**This work**
			O_2	**1452**		
		Ethanol	**Air**	**11076**		
			O2	**13712**		

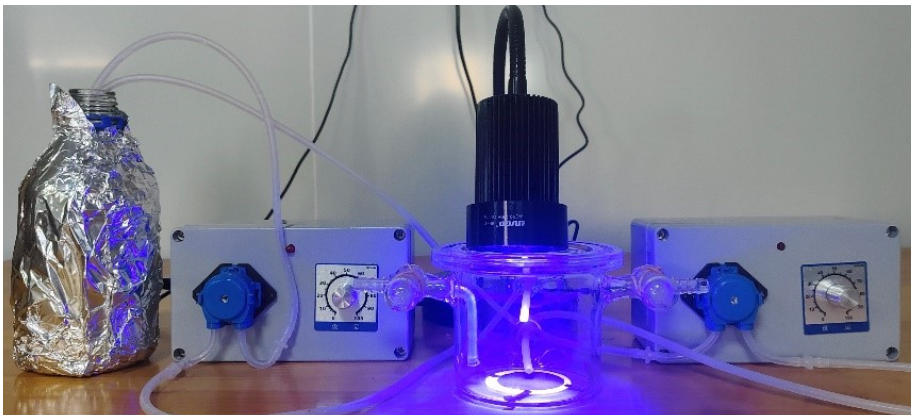

Figure S25. Continuous-flow reactor for H_2O_2 production.

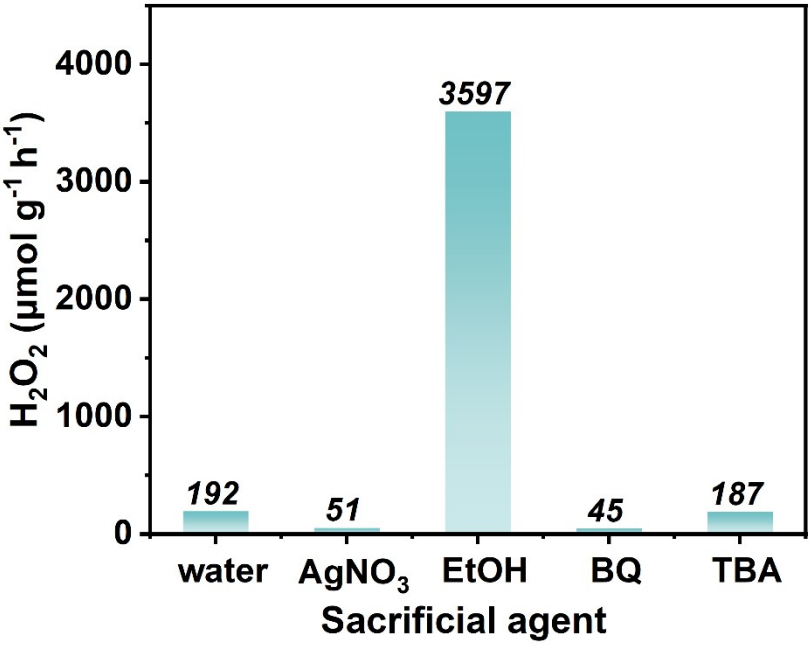

Figure S26. Comparison of H_2O_2 evolution catalyzed by Cd-BTBQ-C with different scavengers ($AgNO_3$, EtOH, BQ and TBA).

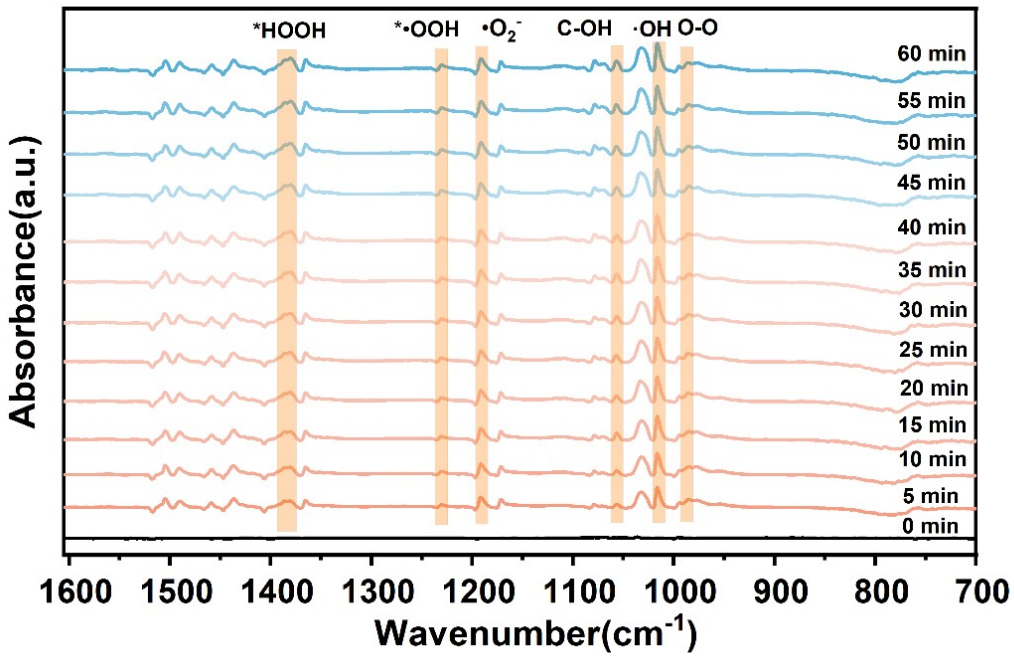

Figure S27. In-situ DRIFTS studies of Cd-BTBQ-N under dark/illuminated conditions.

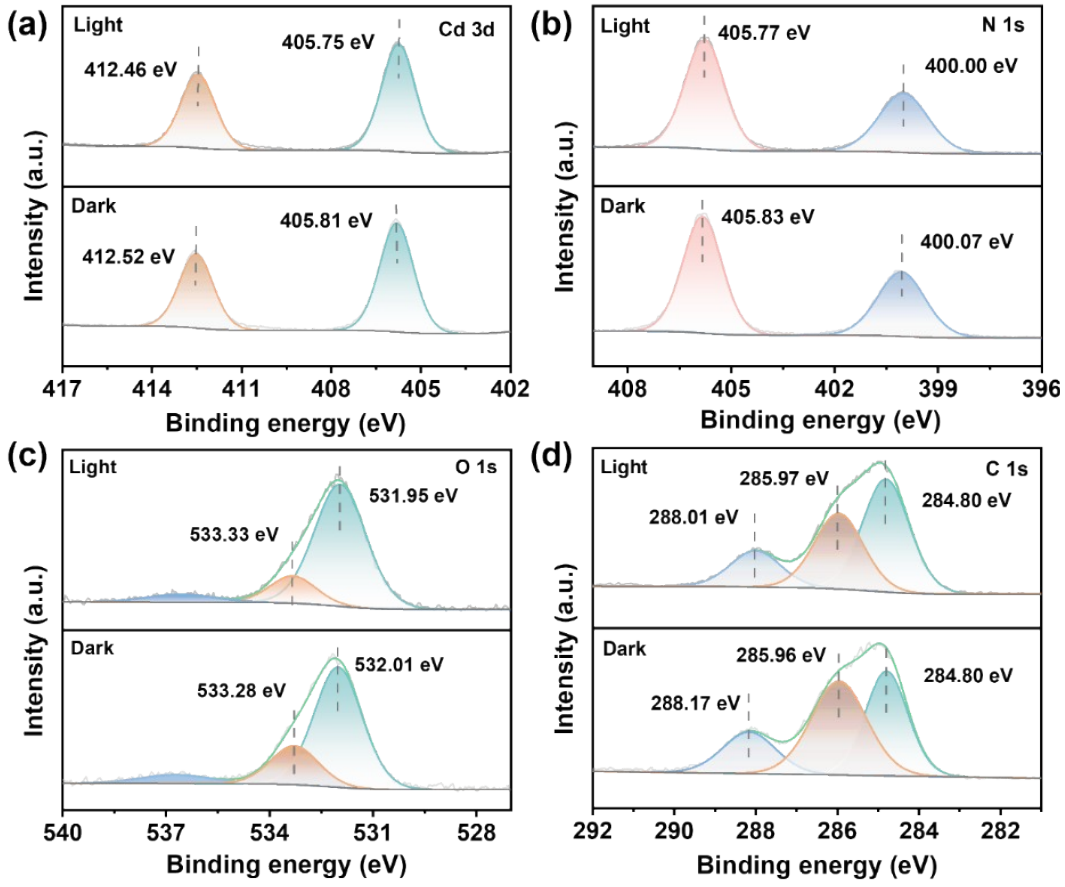

Figure S28. XPS spectra of (a) Cd 3d; (b) N 1s; (c) O 1s and (d) C 1s for Cd-BTBQ-N under dark/illuminated conditions.

References

1. Y. Zheng, H. Zhou, B. Zhou, J. Mao and Y. Zhao, *Catalysis Science & Technology*, 2022, **12**, 969-975.
2. X.-Y. Ji, Y.-Y. Wang, Y. Li, K. Sun, M. Yu and J. Tao, *Nano Research*, 2022, **15**, 6045-6053.
3. Y. Kondo, K. Hino, Y. Kuwahara, K. Mori and H. Yamashita, *Journal of Materials Chemistry A*, 2023, **11**, 9530-9537.
4. Y. Zhao, Y. Liu, J. Cao, H. Wang, M. Shao, H. Huang, Y. Liu and Z. Kang, *Applied Catalysis B: Environmental*, 2020, **278**, 119289.
5. Y. Zhao, Y. Liu, Z. Wang, Y. Ma, Y. Zhou, X. Shi, Q. Wu, X. Wang, M. Shao, H. Huang, Y. Liu and Z. Kang, *Applied Catalysis B: Environmental*, 2021, **289**, 120035.
6. Z. Li, D. Shen, X. Hu, X. Yang, Y. Li and M. Bao, *Chemosphere*, 2023, **343**, 140234.
7. M. Liu, Z. Xing, H. Zhao, S. Song, Y. Wang, Z. Li and W. Zhou, *Journal of Hazardous Materials*, 2022, **437**, 129436.
8. Q. Zhai, Y. Ren, H. Wang, C. Liu, Z. Li and H. Jiang, *Dalton Transactions*, 2024, **53**, 5836-5843.
9. Y. Y. Tang, X. Luo, R. Q. Xia, J. Luo, S. K. Peng, Z. N. Liu, Q. Gao, M. Xie, R. J. Wei, G. H. Ning and D. Li, *Angewandte Chemie International Edition*, 2024, **63**, e202408186.
10. Y. Li, F. Ma, L. Zheng, Y. Liu, Z. Wang, P. Wang, Z. Zheng, H. Cheng, Y. Dai and B. Huang, *Materials Horizons*, 2021, **8**, 2842-2850.
11. X. Chen, Y. Kuwahara, K. Mori, C. Louis and H. Yamashita, *Journal of Materials Chemistry A*, 2021, **9**, 2815-2821.
12. Y. Shen, Y. Yao, L. Lu, C. Zhu, Q. Fang, J. Wang and S. Song, *Chemosphere*, 2023, **324**, 138220.
13. Y. Isaka, Y. Kondo, Y. Kawase, Y. Kuwahara, K. Mori and H. Yamashita, *Chemical Communications*, 2018, **54**, 9270-9273.
14. Y. Wu, X. Li, Q. Yang, D. Wang, F. Yao, J. Cao, Z. Chen, X. Huang, Y. Yang and X. Li, *Chemical Engineering Journal*, 2020, **390**, 124519.
15. J. Wang, Y. Gong, M. Gao, Y. Zheng, Y. Feng, M. Xu, Q. Chu and J. Yan, *ACS Applied Nano Materials*, 2023, **7**, 1067-1077.
16. Y. Kawase, Y. Isaka, Y. Kuwahara, K. Mori and H. Yamashita, *Chemical Communications*, 2019, **55**, 6743-6746.
17. X. Chen, Y. Kuwahara, K. Mori, C. Louis and H. Yamashita, *Journal of Materials Chemistry A*, 2020, **8**, 1904-1910.
18. Y.-C. Hao, L.-W. Chen, J. Li, Y. Guo, X. Su, M. Shu, Q. Zhang, W.-Y. Gao, S. Li, Z.-L. Yu, L. Gu, X. Feng, A.-X. Yin, R. Si, Y.-W. Zhang, B. Wang and C.-H. Yan, *Nature Communications*, 2021, **12**, 2682.
19. Y. Kondo, Y. Kuwahara, K. Mori and H. Yamashita, *The Journal of Physical Chemistry C*, 2021, **125**, 27909-27918.
20. L. Meng, C. Zhao, H. Chu, Y.-H. Li, H. Fu, P. Wang, C.-C. Wang and H. Huang, *Chinese Journal of Catalysis*, 2024, **59**, 346-359.
21. Y.-C. Hao, L.-W. Chen, J. Li, Y. Guo, X. Su, M. Shu, Q. Zhang, W.-Y. Gao, S. Li, Z.-L. Yu, L. Gu, X. Feng, A.-X. Yin, R. Si, Y.-W. Zhang, B. Wang and C.-H. Yan, *Nature Communications*, 2021, **12**, 22991-22997.
22. X. Li, P. Li, Y. Li, H. Liu, Z. Yang, Y. Chen and X. Liao, *Journal of Environmental Chemical Engineering*, 2023, **11**, 110594.
23. Y.-X. Li, Y. Hu, H.-S. Bae, J. Du, S. Zhao, D. Pan and W. Choi, *ACS Nano*, 2024, **18**, 29233-29247.

24. X. Zheng, Z. Pan, J. J. M. Vequizo, R. Yanagi, J. He, A. Yamakata, B. Chen and C. Chu, *Nature Communications*, 2025, **17**, 5422.
25. L. Li, X.-F. Wang, C.-H. Bao, X. Wang, C.-C. Jin, J. Wu, Z. Chen, Y. Yamauchi and Y. S. Ok, *Applied Catalysis B: Environment and Energy*, 2026, **388**, 126555.
26. H. Peng, H. Yang, J. Han, X. Liu, D. Su, T. Yang, S. Liu, C.-W. Pao, Z. Hu, Q. Zhang, Y. Xu, H. Geng and X. Huang, *J Am Chem Soc*, 2023, **145**, 27757-27766.
27. G. Ba, H. Hu, F. Bi, J. Yu, E. Liu, J. Ye and D. Wang, *Applied Catalysis B: Environment and Energy*, 2025, **361**,124645.
28. T. Tian, Q. Shen, Y. Yuan, J. Wang, X. Yang, D. Jiang, C. Zhu, G. Xu and Y. Yuan, *Applied Catalysis B: Environment and Energy*, 2025, **378**, 125567.
29. F. Xue, C. Zhang, H. Peng, L. Sun, X. Yan, F. Liu, W. Wu, M. Liu, L. Liu, Z. Hu, C.-W. Kao, T.-S. Chan, Y. Xu and X. Huang, *Nano Energy*, 2023, **117**, 108902.
30. K. Zhong, G. Wu, P. Sun, S. Chen, X. Dai, J. Yang, H. Li, Z. Mo and H. Xu, *Applied Catalysis B: Environment and Energy*, 2026, **380**,2478.
31. M. Liu, S. Di, H. Qin, P. Chen, Y. Liu, H. Liu, Q. Zhang, Z. Li and S. Zhu, *Journal of Materials Chemistry A*, 2025, **13**, 30642-30651.
32. C. Li, J. Song, X. Guo, R. Zhang, P. Ma and K. Zheng, *Advanced Functional Materials*, 2025, **1**, e25385.
33. T. Mahvelati-Shamsabadi, H. Fattahimoghaddam, B.-K. Lee, H. Ryu and J. I. Jang, *Chemical Engineering Journal*, 2021, **423**, 130067.